

OCCAM

OXFORD CENTRE FOR COLLABORATIVE APPLIED MATHEMATICS

Simulation of cell movement through evolving environment: a fictitious domain approach

by

Jean-Charles Séguis
Kevin Burrage
Radek Erban
David Kay

OCCAM Preprint Number 12/48

Simulation of cell movement through evolving environment: a fictitious domain approach

Jean-Charles Séguis[a,*], Kevin Burrage[b,c], Radek Erban[a], David Kay[c]

[a] *OCCAM, Gibson Building, Mathematical Institute, 2429 St Giles', Oxford OX1 3LB, UK.*
[b] *School of Mathematical Sciences, Queensland University of Technology, Brisbane, Australia.*
[c] *Computational Biology Group, Dept Computer Science, Wolfson Building, Parks Road, Oxford OX1 3QD, UK.*

Abstract

A numerical method for simulating the movement of unicellular organisms which respond to chemical signals is presented. Cells are modelled as objects of finite size while the extracellular space is described by reaction-diffusion partial differential equations. This modular simulation allows the implementation of different models at the different scales encountered in cell biology and couples them in one single framework. The global computational cost is contained thanks to the use of the fictitious domain method for finite elements, allowing the efficient solve of partial differential equations in moving domains. Finally, a mixed formulation is adopted in order to better monitor the flux of chemicals, specifically at the interface between the cells and the extracellular domain.

Keywords: Fictitious-domain method, simulations in biology, hybrid simulations, chemotaxis, signal transduction

*Corresponding author

Email addresses: seguis@maths.ox.ac.uk (Jean-Charles Séguis), kevin.burrage@cs.ox.ac.uk (Kevin Burrage), erban@maths.ox.ac.uk (Radek Erban), dkay@cs.ox.ac.uk (David Kay)

URL: http://www.cs.ox.ac.uk/people/kevin.burrage/ (Kevin Burrage), http://www.maths.ox.ac.uk/people/erban/ (Radek Erban), http://www.cs.ox.ac.uk/people/david.kay/ (David Kay)

1. Introduction

The phenomenon of chemotaxis, that describes the directed movement of cells up (positive chemotaxis) or down (negative chemotaxis) a gradient of concentration of chemicals, is a key component of a great number of biological processes, such as cancer tumour growth and metastasis [27, 19], wound healing [30, 33] or fertilisation of eggs by sperm [10]. Moreover, chemotaxis cannot be dissociated from signal transduction mechanisms which refers to the chemical mechanisms through which extracellular signalling molecules make their way through the cell membrane and translate into actions that will affect the behaviour of the cell.

Very often, this cell-level behaviour leads to macroscopic population-level patterns over length scales of several order of magnitudes the size of a single cell [4]. The understanding of the sensing mechanism through which cells direct their movement is crucial and the object of numerous mathematical and computational modelling.

One of the earliest contribution to the mathematical modelling of chemotaxis is due to Keller and Segel [25]. It consists of a system of two partial differential equations (PDEs) satisfied by the densities of chemoattractant c and of cells n.

$$\partial_t n = D_n \triangle n - \chi(c)\nabla \cdot [n \nabla c], \tag{1}$$

$$\partial_t c = D_c \triangle c - f(c, n). \tag{2}$$

where D_n, D_c are diffusion coefficients, $\chi(c)$ is the chemotactic sensitivity and $f(c, n)$ describes the production, consumption or degradation of the chemotactic signal. This continuum model implicitly assumes that both cells and chemoattractant are present in sufficiently large numbers.

More detailed models describe cells as individual objects. In particular, they are able to incorporate the details of cell movement and signal transduction pathways. Some cells (for example, bacterium *Escherichia coli*) use the "run and tumble" strategy: a cell runs in a chosen direction, then stops for a brief while, reorients itself (tumbling state) and continues running in a new direction [14]. The time spent travelling in the new direction is chosen according to information that the cell acquires about the signal c along its trajectory. In this case, cells can be modelled as point-like objects described by their positions, velocities and internal variables. Internal variables describe main components of the intracellular signal transduction pathway [15]. Large cells, like cellular slime mold *Dictyostelium discoideum* detects

typical differences in signal concentration over its body length [29]. In this case, cells can be better modelled as finite sized objects, because the crucial components of cell's internal state also depend on their positions within the cell [16, 26].

The collective properties of cell populations are determined by the individual-level behaviour. If one is able to relate the coefficients of population-level PDEs (1)–(2) to the parameters of individual-level models, then the population-level PDEs provide an efficient way for determining how the population-level behaviour depends on the individual-level parameters [12]. The connections between individual-level and population-level models have been established for simplified models of bacterial behaviour where cells are modelled as points [14, 15, 36]. For finite-size cells, the population-level equations have been derived for disk-like cells with a simplified description of signal transduction [16] and for the cellular Pots model [1]. Adding more biological details to individual-level models complicates the derivation of coefficients of macroscopic equations. In some cases, one can estimate them from short bursts of appropriately initialized simulations of the individual-level model [13]. However, these computational approaches are only useful when we know the functional form of the macroscopic equations. For more complicated models of chemotaxis, it is not clear whether the population-level description can be reduced to the classical chemotaxis equation (1) with suitably defined coeffiecients [16]. Then the development of efficient simulation techniques for collections of cells is necessary for understanding how individual-based properties influence collective behaviour of unicellular organisms. In this paper, we present such an approach.

We call the presented method hybrid (or multiscale) because it describes different components of the system using different modelling approaches. Hybrid modelling is widespread in biology [18]. In some cases, models with different levels of details are used in different parts of the computational domain [17]. In this paper, we will use the same model in the whole domain, but it will make use of different scales (in terms of size and number) of cells and extracellular chemicals in the system. Such a hybrid model was presented in Ref. [9] where cells are tracked individually and interact with the density of the chemoattractant (cAMP) satisfying the partial differential equation of the same form as (2) where $f(c, n)$ is replaced by a sum of point sink terms $\rho \sum_j \delta_j$, where the position of the sink is determined by the position of a particular cell in the computational domain. A separate set of differential equations governs the internal dynamics of signalling chemicals in

the intracellular space. In the extracellular space, cells are dimensionless and modelled as points. A hybrid model which describes cells as points and external chemicals by PDEs has also been constructed for collections of bacteria in Ref. [12]. In this model, two external signal fields are considered (aspartate and succinate) and coupled with the individual-based model of bacteria *E. coli*. Bacteria are chemotactic towards aspartate. They consume succinate, secrete aspartate and proliferate with doubling time of 2 hours. Succinate-starved cells can also consume aspartate. The population-level behaviour of this hybrid model include travelling waves [5, 35]. Ref. [6] presents a hybrid chemotactic system consisting of cells and oxygen as chemoattractant in which cells have a finite size and therefore not considered as points. The cells, supposed to represent *E. coli*. Bacteria, are propelled by a flagellum and move in a "run and tumble" fashion, however the membrane of cells is not modelled as such, so this model cannot implement the crucial role of the plasma membrane in the signal transduction process.

In this paper, we present an approach to simulating the chemotaxis of cells which is capable to describe the system at both intracellular and extracellular levels. The main feature consists in modelling cells as finite-sized non-deformable[1] solid objects while adopting a continuous approach to model the evolution of the concentration of extracellular chemicals. The simulation framework we present here also allows to implement the modelling of chemical dynamics at three levels in a modular way: intracellular level, at the interface between the intracellular and the extracellular domains and in the extracellular space with possible feedbacks and effects on the motion of cells. This approach can as well accommodate the coupling of spatial extracellular dynamics and spatial intracellular dynamics even if we are not implementing this idea in this paper.

The main challenge consists in making this simulation computationally affordable whilst not compromising on the level of details: this includes differentiating the extracellular and intracellular spaces and modelling the cell membrane governing the exchanges between the bulk and the cytosol. Hence, instead of a volume depletion (or production) term $f(c, n)$, the absorption (or emission) of chemoattractant by the cells will appear as a boundary condition

[1]This is not a requirement, since the framework we present would also work with deformable cells keeping their area constant. However, considering only non-deformable cells simplifies the presentation of our scheme.

at the cells boundary.

Those requirements lead us to solve a reaction-diffusion equation similar to (2) on a deforming domain (the extracellular domain) due to the motion of the cells. In order to make this cost acceptable, our computational model takes advantage of the fictitious domain method for finite elements that allow us to avoid using costly remeshing and interpolations between grids between two time steps. A mixed method is employed that allocate specific degrees of freedom to the flux of chemicals, allowing to better monitor the exchanges between the cytosol and the bulk.

The fictitious domain method is widely used in computational fluid dynamics [8, 20, 21] for the simulation of particulate flows for instance. In spite of the complex geometry of the problem, often posed in a moving domain, fictitious domain method allows the use of a single computational grid for the whole simulation by extending the original domain to a simpler fixed domain. The boundary conditions are then imposed through Lagrange multipliers living on the original boundary or are volume-supported [23]. In terms of numerics, the resulting linear problem is a saddle-point system, which requires adequate preconditioning for optimal performance [3].

The advantages of adopting our approach can be summarised as follows:

- The modelled cells have a finite size, and are not point particles.
- The membrane of cells is modelled mathematically; this allows the accurate modelling of exchanges between the bulk and the cytosol.
- Our simulation framework is highly modular, allowing to couple easily different models of different nature.
- The computational cost of the simulation is contained due to the fictitious domain method. Furthermore, fast numerical techniques can be applied for solving linear systems resulting of the discretisation of PDEs on regular grids.

This paper is organised in the following way: in Section 2, we introduce the various objects of the modelling and write the mathematical formulation of their evolution. In Section 3, we will discuss the numerical discretisation strategy and the computation of fictitious domain specific matrices. Finally in Section 4, we will actually implement the scheme developed in the earlier sections and show some results when simulating a simplified chemotactic system.

2. Mathematical formulation

2.1. Notation and domain definition

Let us define a cavity Ω, a bounded subset of $\mathbb{R}^2$, with a smooth boundary $\partial\Omega$. This domain Ω will be our computational domain, including the interior of the modelled cells. For ease, Ω is taken as a rectangle with dimension $L_1 \times L_2$.

Let $C_i(t)$ be the interior of the i-th modelled cell, for $i = 1, \ldots, N$, where N is the total number of modelled cells (see Figure 1). Hence, at any instant t, the cellular domain is $\mathcal{C}(t) = \bigcup_{j=1}^{N} C_j(t)$ and the extracellular space $\Omega \backslash \overline{\mathcal{C}(t)} = \Omega \setminus \bigcup_{j=1}^{N} \overline{C_j(t)}$. The interface $\mathcal{I}(t) = \bigcup_{j=1}^{N} \partial C_j(t)$ is the frontier between these two. We also denote $\mathcal{I}_j(t) = \partial C_j(t)$. Furthermore, we assume that the modelled cells are bounded and convex.

Let $\boldsymbol{u} = (u_1, u_2, \ldots, u_p)^\top$ with $p \geq 1$ be the vector of densities of p signalling chemicals. The vector $\boldsymbol{u}$ is defined in the spatio-temporal domain $\mathcal{G}$ formed by the successive shapes of the extracellular domain in time, that is to say $\mathcal{G} = \{(\boldsymbol{x}, t) \in \Omega \times [0, T]$ such that $\boldsymbol{x} \notin \overline{\mathcal{C}(t)}\}$.

Let $\boldsymbol{x}_i(t)$, for $i = 1, \ldots, N$ be the position of the centre of mass of cell i at time t, and $\theta_i(t)$ its angle with respect to the horizontal axis (see Figure 2). We also denote $\boldsymbol{v}_i(t)$ its velocity and $\boldsymbol{\omega}_i(t)$ its angular speed. Given that two cells cannot overlap at any instant, the set of positions of the centres of mass of the cells can be written as $\{\{\boldsymbol{x}_i\} \subset \Omega^N$ such that $\text{dist}(C_i(t), C_j(t)) > 0, \forall (i, j), i \neq j\}$.

Finally, we introduce the variable $\boldsymbol{y}_i = (y_1, y_2, \ldots, y_q)^\top \in \mathbb{R}^q$, where $q \geq p$ describing the internal processes undergone in each cell [15]. They can be of different nature, for instance chemical or mechanical. By default, the first p variables of this vector track the intracellular (or membrane-located) densities of the chemical species that are present in the extracellular space. The last $q - p$ variables may represent other species that may be found exclusively intracellularly or on the membrane, for instance signalling receptors and intermediate chemical products on the intracellular signalling pathways.

In the weak formulation of the governing equations introduced in this section, we will make extensive use of classic Lebesgue and Sobolev spaces.

They will be denoted in the following way:

$$\begin{aligned} L^2(\omega) &= \left\{ u : \int_\omega |u|^2 < \infty \right\}, \\ H^1(\omega) &= \left\{ u \in L^2(\omega) : \nabla u \in L^2(\omega)^2 \right\}, \\ \mathcal{H}_{\mathrm{div}}(\omega) &= \left\{ \boldsymbol{\tau} \in L^2(\omega)^2 : \nabla \cdot \boldsymbol{\tau} \in L^2(\omega) \right\}, \\ H_0^1(\omega) &= \left\{ u \in H^1(\omega) : u = 0 \text{ on } \partial\omega \right\}. \end{aligned}$$

2.2. Governing strong equations

2.2.1. Signalling chemicals

We describe the evolution in time and space of the density of signalling chemicals $\boldsymbol{u} = \boldsymbol{u}(\boldsymbol{x}, t)$ by a system of p coupled reaction-advection-diffusion equations. The density of the i-th signalling chemical satisfies the following PDE:

$$\begin{aligned} \partial_t u_i + \boldsymbol{v} \cdot \nabla u_i = \;& d_i \triangle u_i + f_i(\boldsymbol{u}) && \text{in } \mathcal{G}, \\ -d_i \nabla u_i \cdot \boldsymbol{n} = \;& g_i(\boldsymbol{u}) && \text{on } \mathcal{I}_j(t), \forall t \in [0,T] \\ & && \forall j \in \{1, \ldots, N\}, \\ u_i(\cdot, 0) = \;& u_{i0}, && \text{in } \Omega \setminus \mathcal{C}(0), \end{aligned} \tag{RDE}$$

where the symbol d_i represents the diffusion constant of the i-th chemical.

The functions $f_i : \mathbb{R}^p \to \mathbb{R}$ and $g_i : \mathbb{R}^p \to \mathbb{R}$, respectively model the chemical interactions between the p species in the extracellular space and on the membrane of the cells. *A priori*, they could be both nonlinear in $\boldsymbol{u}$.

This reaction-diffusion equation is very similar to (2), except that the influence of the cells does not appear as a volume depletion term, but as a reaction term in the boundary conditions, at the interface between the cells and the extracellular space.

The rate of change of the density u_i is written in a Eulerian frame of reference and the velocity field $\boldsymbol{v}$ characterises the deformation of the extracellular domain. Additional information about the evolution of $\boldsymbol{v}$ is necessary, since the velocity field is only known at the boundary of the cells being $\boldsymbol{v}_i + \boldsymbol{\omega}_i \times (\cdot - \boldsymbol{x}_i)$, $\boldsymbol{v}_i$ being the velocity of the centre of gravity of cell i, $\boldsymbol{\omega}_i$ its angular speed. When decreasing the size of the cells to zero, we expect that the range over which the modulus of velocity field is significant tends to zero as well, so the advection term completely disappears when the cells become point particles.

In Equation (RDE), no boundary condition on $\partial\Omega$ has been provided. This is because appropriate boundary conditions can be imposed that model

various biological situations: Dirichlet or Neumann boundary conditions, periodic boundary conditions.

2.2.2. Velocity field

We assume the extracellular environment can be considered as a Newtonian fluid with density ρ, viscosity ν.

The extracellular domain deforms in time, however, since the area of each cell remains constant in time, the area of the extracellular space is also constant. Therefore the velocity field $\boldsymbol{v}$ is divergence-free.

We assume that the velocity field $\boldsymbol{v}$ satisfies an unsteady Stokes equation, with Dirichlet boundary conditions at the boundary of each cell and at the boundary of the cavity Ω:

$$\begin{aligned} \rho\,\partial_t \boldsymbol{v} &= \nu \triangle \boldsymbol{v} - \nabla p && \text{in } \mathcal{G}, \\ \nabla \cdot \boldsymbol{v} &= 0 && \text{in } \mathcal{G}, \\ \boldsymbol{v} &= \boldsymbol{0} && \text{on } \partial\Omega \times [0,T], \\ \boldsymbol{v} &= \boldsymbol{v}_j + \boldsymbol{\omega}_j \times (\cdot - \boldsymbol{x}_j) && \text{on } \partial C_j(t), \forall t \in [0,T] \\ & && \forall j \in \{1,\dots,N\}. \end{aligned} \tag{STO}$$

Equation (STO) is defined on the same spatio-temporal domain as Equation (RDE). Computationally, this will prove to be of importance later on when discretising the domain $\mathcal{G}$.

Note that the Dirichlet data at the boundary of each cell satisfies the compatibility condition:

$$\int_{\partial C_i(t)} \boldsymbol{v} \cdot \boldsymbol{n}\, \mathrm{d}s = 0, \quad \forall i \in \{1,\dots,N\}, \tag{3}$$

where the normal $\boldsymbol{n}$ points outward of $\mathcal{G}$, *i.e.* inwards each cell.

2.2.3. Description of the motion of cells

To close the description of the whole system (cells + chemicals), it is necessary to provide equations of motion for each cell. Let Δt be some time step, then we write following [34, 7], $\forall i \in \{1,\dots,N\}$:

$$\boldsymbol{x}_i(t+\Delta t) = \boldsymbol{x}_i(t) + \boldsymbol{v}_i(t)\Delta t \tag{4a}$$

$$\boldsymbol{v}_i(t+\Delta t) = \boldsymbol{v}_i(t) + \beta(\boldsymbol{F}_i - \boldsymbol{v}_i(t))\,\Delta t + \beta\sqrt{2D_i\Delta t}\;\xi \tag{4b}$$

$$\boldsymbol{\omega}_i(t+\Delta t) = \boldsymbol{\omega}_i(t) + \boldsymbol{G}_i\,\Delta t, \tag{4c}$$

where

$$\boldsymbol{F}_i = \boldsymbol{F}_i(t, \{\boldsymbol{x}_j(t), \theta_j(t)\}_j, \{\boldsymbol{v}_j(t), \boldsymbol{\omega}_j(t)\}_j, \boldsymbol{y}_i)$$

and

$$\boldsymbol{G}_i = \boldsymbol{G}_i(t, \{\boldsymbol{x}_i(t), \theta_i(t)\}, \{\boldsymbol{v}_i(t), \boldsymbol{\omega}_i(t)\}, \boldsymbol{y}_i)$$

are respectively the force and torque terms acting on each cell. They can include as well repulsive forces allowing to enforce the non-overlapping condition of cells [28]. The parameter D_i represents the diffusion constant of cell i, and β is a scaling parameter. Finally, ξ is a sample from the normal distribution $N(0, 1)$.

Remark 1. *As $\beta \to \infty$, then Equation* (4a) *becomes:*

$$\boldsymbol{x}_i(t + \Delta t) = \boldsymbol{x}_i(t) + \boldsymbol{F}_i \, \Delta t + \sqrt{2D_i \Delta t} \; \xi, \tag{4a'}$$

which can be recognised as a stochastic differential equation (Langevin equation), where $\boldsymbol{F}_i$ is the drift and $\sqrt{2D_i\Delta t}$ the additive noise term.

When simultaneously taking the number N of cells to ∞ and their size to 0, one can recover the partial differential equation satisfied by the density of cells in the Keller-Segel model (1)*, by choosing $\boldsymbol{F}_i = \boldsymbol{F} = \chi(u)\nabla u$.*

Remark 2. *When $D_i = 0$ and as $\Delta t \to 0$, then Equation* (4b) *simply turns into Newton's second law in classical mechanics.*

$$\frac{\mathrm{d}\boldsymbol{x}_i}{\mathrm{d}t}(t) = \boldsymbol{v}_i(t), \tag{4a"}$$

$$\frac{\mathrm{d}\boldsymbol{v}_i}{\mathrm{d}t}(t) = \boldsymbol{F}_i. \tag{4b"}$$

The framework introduced in this section for describing the motion of the cells is very general and allows a wide range of configurations. Other models are also possible, that do not assume a Gaussian behaviour of the random term. In [15, 6], the cells velocity changes by turns randomly, following a Poisson jump process.

2.2.4. Internal dynamics

Following [14], we present a general *black-box* model for the evolution of the vector of internal variables $\boldsymbol{y}$:

$$\frac{\mathrm{d}\boldsymbol{y}}{\mathrm{d}t}(t) = \boldsymbol{I}(t, \boldsymbol{u}, \boldsymbol{y}) \text{ with } \boldsymbol{y}(0) = \boldsymbol{y}_0. \tag{5}$$

The function $\boldsymbol{I}$ encapsulates all the causes of variations for $\boldsymbol{y}(t)$. This function *a priori* depends in a nonlinear fashion on the density of chemicals $\boldsymbol{u}$ in the extracellular space and on the current state of internal variables $\boldsymbol{y}(t)$. Spatial effects are not included in the description of the evolution of the internal states.

Conservation of mass – Intracellular to extracellular exchanges: The vector of internal variables $\boldsymbol{y}$ can also include the same chemical species as in the extracellular space. In that case, the function $\boldsymbol{I}$ can be written as: $\boldsymbol{I}(t, \boldsymbol{u}, \boldsymbol{y}) = \int_{\mathcal{I}(t)} \boldsymbol{g}(\boldsymbol{u})\ \mathrm{d}\gamma + \boldsymbol{I}'(t, \boldsymbol{y})$, where $\boldsymbol{I}'$ is a purely reactive term. This ensures that mass is conserved during transfers between the intracellular and the extracellular spaces.

2.3. Weak formulations and the fictitious domain method

2.3.1. Choice of a fictitious domain

As recalled in the introduction, the fictitious domain method is well adapted to the derivation of weak formulations of time-dependent PDEs that are posed on domains changing shape in time. The approach consists in extending the original domain to a larger simple-shaped domain on which regular meshes can be fitted. The boundary conditions are then imposed through the use of Lagrange multipliers.

In the next paragraphs, we will derive convenient weak formulations taking advantage of the fictitious domain method in order to eliminate of the time-dependent domain $\Omega \setminus \overline{C(t)}$.

A natural choice for the simple-shaped extended domain of the fictitious domain method is the whole rectangular cavity Ω. To avoid complicated notation, the extensions to Ω of all unknowns will be denoted by the same symbol as their original counterpart.

2.3.2. Weak form for the reaction-advection-diffusion equation (RDE)

The approach we are adopting is inspired by Joly and Rhaouti [24]. Indeed, the boundary conditions at the boundary of the cells is of Neumann

type, therefore it seems natural to introduce the new variable $\boldsymbol{\sigma}_i$ defined by:

$$\boldsymbol{\sigma}_i = -d_i \nabla u_i \quad \text{in } \mathcal{G}. \tag{6}$$

Then the Neumann boundary condition becomes a Dirichlet boundary condition for $\boldsymbol{\sigma}$. The following weak formulation is derived for $\boldsymbol{\sigma}_i \in \mathcal{H}_{\text{div}}(\Omega)$ by applying the method developed in [24].

In the original domain, the solution of the reaction-advection-diffusion equation should lie in $H^1(\mathcal{G}(t))$. However, with the extension of the domain to Ω, the extended solution u_i becomes discontinuous on the interface, so the extended solution only lies in a broken space $H^1_B(\Omega)$ defined as follows:

$$H^1_B(\Omega) = \left\{ u \in L^2(\Omega) : \ u|_{\Omega \setminus \overline{\mathcal{C}}} \in H^1(\Omega \setminus \overline{\mathcal{C}}) \ \& \ u|_{\mathcal{C}} \in H^1(\mathcal{C}) \right\} \tag{7}$$

However, in this formulation, the normal component of the flux, $\boldsymbol{\sigma} \cdot \boldsymbol{n}$, across the interfaces $\mathcal{I}(t) = \bigcup_{j=1}^{N} \partial C_j(t)$ will remain continuous.

This fact shows that this formulation allows us to simultaneously control the flux of chemicals through the interface (representing the membrane of the cells) and conserve mass of chemicals in the system { bulk + cells }. This would not be possible using a fictitious domain method based on Lagrange elements.

The fictitious weak formulation of Equation (6) reads:

$$\int_\Omega d_i^{-1} \boldsymbol{\sigma}_i \cdot \boldsymbol{\tau} \, \mathrm{d}\Omega + \int_\Omega u_i \, \mathrm{div}\, \boldsymbol{\tau} \, \mathrm{d}\Omega + \sum_{j=1}^{N} \langle \lambda_i, \boldsymbol{\tau} \cdot \boldsymbol{n} \rangle_{\partial C_j(t)} = 0, \quad \forall \tau \in \mathcal{H}_{\text{div}}(\Omega), \tag{8}$$

where $\lambda_i \in H^{1/2}(\mathcal{I}(t))$ represents the jump of u_i across the interface $\mathcal{I}(t) = \bigcup_{j=1}^{N} \partial C_j(t)$, that is to say:

$$\lambda_i(\cdot) = \lim_{\epsilon \to 0} \left[u_i(\cdot + \epsilon \boldsymbol{n}(\cdot)) - u_i(\cdot - \epsilon \boldsymbol{n}(\cdot)) \right]. \tag{9}$$

Then the weak formulation of Problem (RDE) is written:
find $(u_i(\cdot,t), \boldsymbol{\sigma}_i(\cdot,t), \lambda_i(\cdot,t)) \in L^2(\Omega) \times \mathcal{H}_{\text{div}}(\Omega) \times H^{1/2}(\mathcal{I}(t))$ such that $\forall (w, \boldsymbol{\tau}, \mu) \in$

$L^2(\Omega) \times \mathcal{H}_{\mathrm{div}}(\Omega) \times H^{1/2}(\mathcal{I}(t))$,

$$\int_\Omega d_i^{-1}\boldsymbol{\sigma}_i \cdot \boldsymbol{\tau}\ \mathrm{d}\Omega + \int_\Omega u_i \,\mathrm{div}\,\boldsymbol{\tau}\ \mathrm{d}\Omega + \sum_{j=1}^{N} \langle \lambda_i, \boldsymbol{\tau}\cdot\boldsymbol{n}\rangle_{\partial C_j(t)} = 0, \tag{10a}$$

$$\int_\Omega d_i^{-1}\boldsymbol{\sigma}_i \cdot (\boldsymbol{v}w) + \mathrm{div}\,\boldsymbol{\sigma}_i\, w\ \mathrm{d}\Omega + \int_\Omega \partial_t u_i\, w\ \mathrm{d}\Omega = \int_\Omega f(\boldsymbol{u})\, w\ \mathrm{d}\Omega, \tag{10b}$$

$$\sum_{j=1}^{N} \langle \mu, \boldsymbol{\sigma}_i\cdot\boldsymbol{n} - g(\boldsymbol{u})\rangle_{\partial C_j(t)} = 0. \tag{10c}$$

In Equation (10b), $\boldsymbol{v}$ has been extended to Ω so this motivates the usage of the fictitious domain formulation for Problem (STO) in Ω.

2.3.3. Weak form for the unsteady Stokes equation (STO)

The approach we adopt here applies the fictitious domain method for elliptic Dirichlet problems by Glowinski [21]. We extend the velocity field $\boldsymbol{v}$ to the whole of Ω. The Dirichlet boundary conditions at the boundary of each cell are then imposed using a Lagrange multiplier $\boldsymbol{\xi}$.

Other methods are possible, for instance, in [22, 20], by imposing rigid-body motion to the fluid 'filling' the objects modelling the cells. The Lagrange multiplier imposing this motion is then distributed in the volume occupied by the cells. This is convenient when wishing to implement a two-way coupling between the solid objects and the fluid. In our case, since the cells are not inert objects but self-propelled, the action of the fluid on the cells has no relevance. We will therefore assume that the motion of cells is not influenced by viscous drag due to the fluid.

The fictitious weak formulation of Problem (STO) reads:
find $(\boldsymbol{v}(\cdot,t), p, \boldsymbol{\xi}(\cdot,t)) \in H_0^1(\Omega)^2 \times L_0^2(\Omega) \times H^{-1/2}(\mathcal{I}(t))^2$ such that $(\boldsymbol{w}, q, \boldsymbol{\zeta}) \in H_0^1(\Omega)^2 \times L_0^2(\Omega) \times H^{-1/2}(\mathcal{I}(t))^2$,

$$\int_\Omega \rho\,\partial_t \boldsymbol{v}\,\boldsymbol{w} + \nu \boldsymbol{\nabla}\boldsymbol{v} : \boldsymbol{\nabla}\boldsymbol{w}\ \mathrm{d}\Omega - \int_\Omega p\,\mathrm{div}\,\boldsymbol{w}\ \mathrm{d}\Omega + \sum_{j=1}^{N} \langle \boldsymbol{w}, \boldsymbol{\xi}\rangle_{\partial C_j(t)} = 0 \tag{11a}$$

$$\int_\Omega q\,\mathrm{div}\,\boldsymbol{v}\ \mathrm{d}\Omega = 0 \tag{11b}$$

$$\sum_{j=1}^{N} \langle \boldsymbol{v} - (\boldsymbol{v}_j + \boldsymbol{\omega}_j \times (\cdot - \boldsymbol{x}_j)), \boldsymbol{\zeta}\rangle_{\partial C_j(t)} = 0, \tag{11c}$$

where ':' represents the double-dot product. In Equation (11a), since the velocity field $\boldsymbol{v}$ is divergence-free and in $H_0^1(\Omega)^2$, then we can take advantage of the fact that:

$$\int_\Omega \nu \boldsymbol{\nabla v} : \boldsymbol{\nabla w} \, \mathrm{d}\Omega = \int_\Omega 2\nu \boldsymbol{D}[\boldsymbol{v}] : \boldsymbol{D}[\boldsymbol{w}] \, \mathrm{d}\Omega, \quad \forall \boldsymbol{w} \in H_0^1(\Omega)^2 \tag{12}$$

where $\boldsymbol{D}[\boldsymbol{v}] = \frac{1}{2}(\boldsymbol{\nabla v} + \boldsymbol{\nabla v}^\top)$ is the rate-of-strain tensor.

The Lagrange multiplier $\boldsymbol{\xi}$ can be interpreted as the jump of the quantity $2\nu \boldsymbol{D}[\boldsymbol{v}](\boldsymbol{n}) + p\boldsymbol{n}$ across the interface $\partial C_j(t)$, where $\boldsymbol{n}(\cdot)$ is the local outward normal at the interface $\mathcal{I}(t)$.

In this formulation, we can see that the extended solution $\boldsymbol{v}$ is expected to be continuous across the interfaces ∂C_j, for all j. It will therefore be continuous on $\overline{\Omega}$, hence element of $L^\infty(\Omega)$. This ensures that the advection term of Equation (10b) is well-defined.

3. Computational scheme

3.1. Spatial discretisation

The main advantage of the fictitious domain method is to allow the use of regular meshes. We opt for a triangulation $\mathcal{T}_h$ obtained from a rectangular mesh of $(2k_1 - 1) \times (2k_2 - 1)$ vertices, by subdividing each square into two triangles with their diagonal of negative slope. We also assume that the mesh size satisfies $h = \frac{L_1}{2k_1-1} = \frac{L_2}{2k_2-1}$.

We define a self-similar triangulation with mesh size $2h$, labelled $\mathcal{T}_{2h}$. Figure 3 shows the two triangulations.

Thirdly, the domain formed by the union of the interfaces $\mathcal{I}(t) = \bigcup_{j=1}^N \mathcal{I}_j(t)$ must also be discretised. Let η the mesh size of the discretised interface. The interface is then divided in $|\mathcal{I}(t)|/\eta$ segments of equal length. We further assume, for stability reasons, that $h = \alpha\eta$, where $\alpha \in [0.5, 1]$. See [24] for more details. The mesh size of the interface is then coarser than that of the cavity.

When refining the main mesh *i.e.* reducing h, it is likely that we will have to reduce η by the same factor, therefore making η dependent of h. For that reason, the approximation spaces for the Lagrange multipliers instead of bearing a η subscript will bear a h subscript instead. We denote $\mathcal{I}_h$ the set of segments forming the discretised interface.

We can then define the approximation spaces linked to those triangulations. For Problem (10), we introduce first order Raviart-Thomas elements

$RT_0(\Omega)$ [31] and piecewise linear elements for the Lagrange multiplier space:

$$\boldsymbol{V}_h = \left\{\boldsymbol{\tau}_h \in \mathcal{H}_{\mathrm{div}}(\Omega) \cap C(\overline{\Omega})^2 \mid \forall K \in \mathcal{T}_h,\ \ \boldsymbol{\tau}_h|_K(\cdot) = \boldsymbol{a} + b \cdot \right. \\ \left. \text{and } \forall E \in \mathcal{E}_{\mathcal{T}_h},\ [\boldsymbol{\tau}_h]_E = 0\right\}, \tag{13a}$$

$$M_h = \left\{q \in L^2(\Omega) \cap C(\overline{\Omega}) \mid \forall T \in \mathcal{T}_h,\ \ q|_T \in P_0\right\}, \tag{13b}$$

$$\Lambda_h = \left\{\lambda \in H^{1/2}(\mathcal{I}(t)) \cap C(\overline{\mathcal{I}(t)}) \mid \forall I \in \mathcal{I}_h,\ \ \lambda|_I \in P_0\right\}, \tag{13c}$$

and for Problem (11), we use first order Lagrange elements coupled with discontinuous piecewise constant elements for the pressure. The Lagrange multiplier space is discretised in piecewise discontinuous constant elements:

$$\boldsymbol{W}_h = \left\{\boldsymbol{w}_h \in H_0^1(\Omega)^2 \cap C(\overline{\Omega})^2 \mid \forall T \in \mathcal{T}_h,\ \ \boldsymbol{w}_h|_T \in P_2 \times P_2\right\}, \tag{14a}$$

$$Q_h = \left\{q \in L_0^2(\Omega) \cap C(\overline{\Omega}) \mid \forall T \in \mathcal{T}_{2h},\ \ q|_T \in P_1 \text{ and } \int_\Omega q \,\mathrm{d}\Omega = 0\right\}, \tag{14b}$$

$$\boldsymbol{\Xi}_h = \left\{\boldsymbol{\zeta} \in H^{-1/2}(\mathcal{I}(t))^2 \cap C(\overline{\mathcal{I}(t)})^2 \mid \forall I \in \mathcal{I}_h,\ \ \boldsymbol{\zeta}|_I \in P_0 \times P_0\right\}. \tag{14c}$$

In the above definitions, P_0 denotes the constants and P_1 the space of linear polynomials.

3.2. Finite element formulations

Using the definition of the finite element approximation spaces in the previous section, we write the finite element formulation of (RDE) and (STO).

3.2.1. F.E. formulation of the reaction-advection-diffusion equation (RDE)

Find $(u_{i,h}(\cdot,t), \boldsymbol{\sigma}_{i,h}(\cdot,t), \lambda_{i,h}(\cdot,t)) \in \boldsymbol{V}_h \times M_h \times \Lambda_h$ such that $\forall (w_h, \boldsymbol{\tau}_h, \mu_h) \in \boldsymbol{V}_h \times M_h \times \Lambda_h$,

$$\int_\Omega d_i^{-1} \boldsymbol{\sigma}_{i,h} \cdot \boldsymbol{\tau}_h \,\mathrm{d}\Omega + \int_\Omega u_{i,h} \,\mathrm{div}\, \boldsymbol{\tau}_h \,\mathrm{d}\Omega + \sum_{j=1}^{N} \int_{\mathcal{I}_j(t)} \lambda_{i,h} \left(\boldsymbol{\tau}_h \cdot \boldsymbol{n}\right) \mathrm{d}\mathcal{I}_j(t) = 0, \tag{15a}$$

$$\int_\Omega d_i^{-1} \boldsymbol{\sigma}_{i,h} \cdot (\boldsymbol{v} w_h) + \mathrm{div}\, \boldsymbol{\sigma}_{i,h}\, w_h \,\mathrm{d}\Omega + \int_\Omega \partial_t u_{i,h}\, w_h \,\mathrm{d}\Omega = \int_\Omega f_i(\boldsymbol{u}_h)\, w_h \,\mathrm{d}\Omega, \tag{15b}$$

$$\sum_{j=1}^{N} \int_{\mathrm{d}\mathcal{I}_j(t)} \mu_h \left(\boldsymbol{\sigma}_{i,h} \cdot \boldsymbol{n} - g_i(\boldsymbol{u}_h)\right) \mathrm{d}\mathcal{I}_j(t) = 0. \tag{15c}$$

3.2.2. F.E. formulation of the unsteady Stokes equation (STO)

Find $(\boldsymbol{v}_h(\cdot,t), p_h(\cdot,t), \boldsymbol{\xi}_h(\cdot,t)) \in \boldsymbol{W}_h \times Q_h \times \boldsymbol{\Xi}_h$ such that $(\boldsymbol{w}_h, q_h, \boldsymbol{\zeta}_h) \in \boldsymbol{W}_h \times Q_h \times \boldsymbol{\Xi}_h$,

$$\int_\Omega \rho\, \partial_t \boldsymbol{v}_h\, \boldsymbol{w}_h + \nu \boldsymbol{\nabla} \boldsymbol{v}_h : \boldsymbol{\nabla} \boldsymbol{w}_h \, \mathrm{d}\Omega - \int_\Omega p_h \operatorname{div} \boldsymbol{w}_h \, \mathrm{d}\Omega + \sum_{j=1}^{N} \int_{\mathcal{I}_j(t)} \boldsymbol{w}_h \cdot \boldsymbol{\xi}_h \, \mathrm{d}\mathcal{I}_j(t) = 0 \tag{16a}$$

$$\int_\Omega q_h \operatorname{div} \boldsymbol{v}_h \, \mathrm{d}\Omega = 0 \tag{16b}$$

$$\sum_{j=1}^{N} \int_{\mathcal{I}_j(t)} (\boldsymbol{v}_h - \pi_h(\boldsymbol{v}_j + \boldsymbol{\omega}_j \times (\cdot - \boldsymbol{x}_j))) \cdot \boldsymbol{\zeta}_h \, \mathrm{d}\mathcal{I}_j(t) = 0, \tag{16c}$$

where, in (16c), π_h is the projection operator on the $H^{1/2}(\mathcal{I}(t))$.

Here, the numerical solution of (16), $\boldsymbol{v}_h$, is element of $H_0^1(\Omega)^2$. However, when looking carefully at Equation (15b), it would be convenient to work with the projection of the flow in $\mathcal{H}_{\mathrm{div}}(\Omega)$, so a flow in $\boldsymbol{W}_h = RT_0(\Omega)$. In this case, we can use the classic projection operator from $H^1(\Omega)^2$ to $\boldsymbol{W}_h$ defined as follows:

$$\pi_h(\boldsymbol{v}_h) = \sum_{e \in \mathcal{E}} \left(\int_e \boldsymbol{v}_h \cdot \boldsymbol{\tau}_e \, \mathrm{d}s \right) \boldsymbol{\tau}_e, \tag{17}$$

where $\boldsymbol{\tau}_e \in \boldsymbol{W_h}$ satisfies $\boldsymbol{\tau}_e \cdot \boldsymbol{n}_e = 1$ on e.

3.3. Temporal scheme

Let $\Delta t > 0$ be the constant time step used for the temporal discretisation of Problems (RDE), (STO) and (4). We denote the value at time $t_k = k\Delta t$ of any quantity q_h as $q_h(k\Delta t) = q_h^k$.

3.3.1. Reaction-advection-diffusion equation: an operator-splitting approach

Operator splitting is a popular method to solve the reaction-advection-diffusion problem because it allows to cope with various difficulties, advection dominated problem, stiff reaction term for instance, by splitting the problem into simpler components and addressing each of them accurately.

We use a simple first-order accurate two-step operator-splitting scheme to compute the update $u_{i,h}^{k+1}$ from the previously computed $u_{i,h}^{k}$. First, we compute the update $u_{i,h}^{k+1/2}$ from an advection step and then $u_{i,h}^{k+1}$ using the intermediary update $u_{i,h}^{k+1/2}$ from the diffusion step. To sum up:

1. $\dfrac{u_{i,h}^{k+1/2} - u_{i,h}^{k}}{\Delta t} + \boldsymbol{v}_h^{k+1} \cdot \nabla u_{i,h}^{k+1/2} = 0,$

2. $\dfrac{u_{i,h}^{k+1} - u_{i,h}^{k+1/2}}{\Delta t} - d_i \triangle u_{i,h}^{k+1} = f(u_{i,h}^{k+1})$ with $d_i \nabla u_{i,h}^{k+1} \cdot \boldsymbol{n} = g_i(u_{i,h}^{k+1}).$

In the first step, no boundary condition need to be imposed since there is no flow in or out of the cavity Ω. Moreover, since there is no convective flux in or out the cells, no boundary condition is imposed at the interface between cells and the extracellular space. So the advection step is taken in the whole of Ω.

Lastly, for stability reasons, we penalise the advection term with a $\epsilon-$sized diffusion term, where $\epsilon = \mathcal{O}(h)$.

The update $u_{i,h}^{k+1/2}$ is then the solution of:
Find $\left(\boldsymbol{\sigma}_{i,h}^{k+1/2}, u_{i,h}^{k+1/2}\right) \in \boldsymbol{V}_h \times M_h$ such that $\forall (w_h, \boldsymbol{\tau}_h) \in \boldsymbol{V}_h \times M_h$ and given $u_{i,h}^{k} \in_h M_h$,

$$\int_\Omega \epsilon^{-1} \boldsymbol{\sigma}_{i,h}^{k+1/2} \cdot \boldsymbol{\tau}_h \, \mathrm{d}\Omega - \int_\Omega u_{i,h}^{k+1/2} \mathrm{div}\, \boldsymbol{\tau}_h \, \mathrm{d}\Omega = 0, \tag{18a}$$

$$\int_\Omega \left(\epsilon^{-1} \boldsymbol{\sigma}_{i,h}^{k+1/2} \cdot \boldsymbol{v}_h^{k+1} + \mathrm{div}\, \boldsymbol{\sigma}_{i,h}^{k+1/2}\right) w_h \, \mathrm{d}\Omega + \int_\Omega \frac{u_{i,h}^{k+1/2} - u_{i,h}^{k}}{\Delta t} w_h \, \mathrm{d}\Omega = 0. \tag{18b}$$

The second step of the operator-splitting scheme is written:
Find $\left(\boldsymbol{\sigma}_{i,h}^{k+1}, u_{i,h}^{k+1}, \lambda_{i,h}^{k+1}\right) \in \boldsymbol{V}_h \times M_h \times \Lambda_h$ such that $\forall (\boldsymbol{\tau}_h, w_h, \mu_h) \in \boldsymbol{V}_h \times$

$M_h \times \Lambda_h$ and given $u_{i,h}^{k+1/2} \in M_h$,

$$\int_\Omega d_i^{-1} \boldsymbol{\sigma}_{i,h}^{k+1} \cdot \boldsymbol{\tau}_h \, \mathrm{d}\Omega - \int_\Omega u_{i,h}^{k+1} \mathrm{div}\, \boldsymbol{\tau}_h \, \mathrm{d}\Omega + \sum_{j=1}^{N} \int_{\mathcal{I}_j(t)} \lambda_{i,h}^{k+1} (\boldsymbol{\tau}_h \cdot \boldsymbol{n}) \, \mathrm{d}\mathcal{I}_j(t) = 0, \tag{19a}$$

$$\int_\Omega \mathrm{div}\, \boldsymbol{\sigma}_{i,h}^{k+1} w_h \, \mathrm{d}\Omega + \int_\Omega \frac{u_{i,h}^{k+1} - u_{i,h}^{k+1/2}}{\Delta t} \, w_h \, \mathrm{d}\Omega = \int_\Omega f_i(u_{i,h}^{k+1}) \, w_h \, \mathrm{d}\Omega, \tag{19b}$$

$$\sum_{j=1}^{N} \int_{\mathcal{I}_j(t)} \mu_h \left(\boldsymbol{\sigma}_{i,h}^{k+1} \cdot \boldsymbol{n} - g_i(\boldsymbol{u}_h^{k+1}) \right) \mathrm{d}\mathcal{I}_j(t) = 0. \tag{19c}$$

3.3.2. Unsteady stokes problem

Let us integrate (16) between $t_k = k\,\Delta t$ and $t_{k+1} = (k+1)\,\Delta t$ and adopt a fully implicit scheme. No splitting is necessary here. Find $(\boldsymbol{v}_h^{k+1}, p_h^{k+1}, \boldsymbol{\xi}_h^{k+1}) \in \boldsymbol{W}_h \times Q_h \times \boldsymbol{\Xi}_h$ such that $(\boldsymbol{w}_h, q_h, \boldsymbol{\zeta}_h) \in \boldsymbol{W}_h \times Q_h \times \boldsymbol{\Xi}_h$,

$$\int_\Omega \frac{\rho}{\Delta t} \, \boldsymbol{v}_h^{k+1} \, \boldsymbol{w}_h + \nu \boldsymbol{\nabla} \boldsymbol{v}_h^{k+1} : \boldsymbol{\nabla} \boldsymbol{w}_h \, \mathrm{d}\Omega - \int_\Omega p_h^{k+1} \, \mathrm{div}\, \boldsymbol{w}_h \, \mathrm{d}\Omega + \sum_{j=1}^{N} \int_{\mathcal{I}_j^{k+1}} \boldsymbol{w}_h \cdot \boldsymbol{\xi}_h^{k+1} \, \mathrm{d}\mathcal{I}_j^{k+1} = \int_\Omega \frac{\rho}{\Delta t} \, \boldsymbol{v}_h^k \, \boldsymbol{w}_h \, \mathrm{d}\Omega, \tag{20a}$$

$$\int_\Omega q_h \, \mathrm{div}\, \boldsymbol{v}_h^{k+1} \, \mathrm{d}\Omega = 0, \tag{20b}$$

$$\sum_{j=1}^{N} \int_{\mathcal{I}_j^{k+1}} \left(\boldsymbol{v}_h^{k+1} - \pi_h(\boldsymbol{v}_j + \boldsymbol{\omega}_j \times (\cdot - \boldsymbol{x}_j)) \right) \cdot \boldsymbol{\zeta}_h \, \mathrm{d}\mathcal{I}_j^{k+1} = 0. \tag{20c}$$

3.3.3. Matrix form of the discretised equations

The discretised sets of equations (18) and (20) can be written in the form of linear sets of equations. The matrix form of the linear systems of the two-step operator splitting scheme (18)-(19) can be formulated as:

$$\begin{bmatrix} \epsilon^{-1} A_1 & B_1^\top \\ B_1 + \epsilon^{-1} C^{k+1} & -\frac{1}{\Delta t} M \end{bmatrix} \begin{bmatrix} \Sigma_i^{k+1/2} \\ U_i^{k+1/2} \end{bmatrix} = \begin{bmatrix} 0 \\ -\frac{1}{\Delta t} M_1 U_i^k \end{bmatrix} \tag{21a}$$

$$\begin{bmatrix} d_i^{-1} A_1 & B_1^\top & (L^k)^\top \\ B_1 & -\frac{1}{\Delta t} M & 0 \\ L^k & 0 & 0 \end{bmatrix} \begin{bmatrix} \Sigma_i^{k+1} \\ U_i^{k+1} \\ \Lambda_i^{k+1} \end{bmatrix} = \begin{bmatrix} 0 \\ -\frac{1}{\Delta t} M_1 U_i^{k+1/2} + F(U_i^{k+1}) \\ G(U_i^{k+1}) \end{bmatrix} \tag{21b}$$

where $A_{1ij} = \int_\Omega \boldsymbol{\tau}_i \cdot \boldsymbol{\tau}_j \,\mathrm{d}\Omega$, $B_{1ij} = \int_\Omega w_j \,\mathrm{div}\, \boldsymbol{\tau}_j \,\mathrm{d}\Omega$, $L^k_{ij} = \sum_{j=1}^N \int_{\mathcal{I}^k_j} \mu_i \,\boldsymbol{\tau}_j \cdot \boldsymbol{n} \,\mathrm{d}\mathcal{I}^k_j$, $M_{1ij} = \int_\Omega w_i \, w_j \,\mathrm{d}\Omega$ and $C^k_{ij} = \int_\Omega \boldsymbol{\tau_j} \cdot (\boldsymbol{v}^k w_i) \,\mathrm{d}\Omega$.

The linearised system (20) is also formulated as:

$$\begin{bmatrix} \nu A_2 + \frac{1}{\Delta t} M_2 & B_2^\top & (X^{k+1})^\top \\ B_2 & 0 & 0 \\ X^{k+1} & 0 & 0 \end{bmatrix} \begin{bmatrix} V^{k+1} \\ P^{k+1} \\ \Xi^{k+1} \end{bmatrix} = \begin{bmatrix} \frac{1}{\Delta t} V^k \\ 0 \\ W^{k+1} \end{bmatrix}, \qquad (22)$$

where $A_{2ij} = \int_\Omega \boldsymbol{\nabla} \boldsymbol{w}_i : \boldsymbol{\nabla} \boldsymbol{w}_j \,\mathrm{d}\Omega$, $M_{2ij} = \int_\Omega \boldsymbol{w}_i \cdot \boldsymbol{w}_j \,\mathrm{d}\Omega$, $B_{2ij} = \int_\Omega q_j \,\mathrm{div}\, \boldsymbol{w}_j \,\mathrm{d}\Omega$ and finally $X^k_{ij} = \sum_{j=1}^N \int_{\mathcal{I}^k_j} \boldsymbol{\mu}_i \cdot \boldsymbol{w}_j \,\mathrm{d}\mathcal{I}^k_j$.

In the case of general nonlinear reaction terms, classical methods for the numerical approximation of solutions of nonlinear ODEs can be used such as Runge-Kutta for instance.

4. Implementation

In this section, we are going to apply the computational method discussed in the previous section to a simplified chemotactic system, first with only one cell and later on, with several dozens of cells. We will show some numerical results that give empirical proof of the stability of the computational method presented here.

4.1. Numerical simulation of the motion of single cell subject to chemotaxis

The objective of this test problem is to simulate the motion of a single cell undergoing chemotaxis in a periodic domain along the x-axis, by a single chemoattractant species subject to diffusion.

This chemoattractant is also absorbed by the cell, which determines the direction of the motion by measuring the concentration of chemoattractant on its membrane. Arbitrarily, the shape of the cell is chosen to be elliptic with major and minor axis a and $b = \frac{a}{2}$ respectively, so the cell has no circular symmetry.

The concentration of chemoattractant $u := u_1$ satisfies (RDE) with $f(u) = 0$ and $g(u) = -ku$, where k is the rate of absorption of the chemoattractant by the cell membrane. The model we adopt for the internal variables of the cell is the "cartoon model" from [14], capturing the main dynamics of the signal transduction process by the cell. This linear models comprises two

variables y_1 and y_2 depending on s the location on the membrane of the cell and t, the time. It satisfies:

$$\frac{\mathrm{d}}{\mathrm{d}t}\begin{pmatrix} t_e\, y_1 \\ t_a\, y_2 \end{pmatrix} = \begin{pmatrix} -1 & 1 \\ 0 & -1 \end{pmatrix}\begin{pmatrix} y_1 \\ y_2 \end{pmatrix} + u(\gamma(s))\begin{pmatrix} 1 \\ 1 \end{pmatrix}. \tag{23}$$

The parameter t_a described the period of adaptation of the cell to the signal u. Roughly speaking, the variable y_2 follows the signal u with a lag of t_a, whereas in the limit of $t_e \ll t_a$, y_1 follows the difference between u and y_2, that is to say: $y_1(s,t) = u(\gamma(s),t) - y_2(s,t)$.

The cell motion is governed by the simplest version of Equations (4), that is to say when there is no random term and parameter $\beta \to \infty$. We introduce the quantity $\boldsymbol{gd}(t)$, the gradient of chemoattractant measured by the cell:

$$\boldsymbol{gd}(t) = \int_{\mathcal{I}(t)} y_1(s,t)\, \boldsymbol{n}(s)\, \mathrm{d}\mathcal{I}(t). \tag{24}$$

The only force acting on the cell is then defined by:

$$\boldsymbol{F}(t,\boldsymbol{y}) = \bar{s}\, \frac{\boldsymbol{gd}(t)}{\epsilon_s + \|\boldsymbol{gd}(t)\|}, \tag{25}$$

where $\boldsymbol{n}$ is the normal at point s of the membrane pointing outwards, $\bar{s}$ the maximum velocity at which a cell can travel and ϵ_s the sensitivity of the cell to the gradient of chemoattractant. This force models the trend for a cell to move towards area of higher concentration of chemoattractant.

The position of the cell and its angle at time $t + \Delta t$ are then given by:

$$\boldsymbol{x}(t+\Delta t) = \boldsymbol{x}(t) + \Delta t\, \boldsymbol{F}(t,\boldsymbol{y}), \tag{26a}$$

$$\theta(t+\Delta t) = \theta(t) + \frac{\Delta t}{T}\left(\arg \boldsymbol{gd}(t) - \theta(t)\right). \tag{26b}$$

Having described entirely the system with evolution equations, we now list below the values of the parameters used in the simulations.

- The unit of length is 1 m.
- The unit of time is 1 min.
- The computational domain Ω is $(0, 1.5) \times (0, 0.25)$.
- The number of chemotactic species is $p = 1$.

- The diffusion constant of the chemoattractant is taken as $d = 5 \times 10^{-2}\,\mathrm{mm}^2.\mathrm{min}^{-1}$.
- The number of cells is $N = 1$.
- The size of the cell [2] is set to $3 \times 10^{-2}\,\mathrm{mm}$. We set the major axis of the cell a to 1.5×10^{-2}.
- The maximum velocity reached by a cell [2] is $\bar{s} = 2 \times 10^{-2}\,\mathrm{mm.min}^{-1}$.
- The sensitivity of the cell to the gradient of chemoattractant is fixed to 10^{-3}.
- The diffusion constant of the cell, D_1, is 0.
- The relaxation constant for the alignment of the cell main axis is $T = 1\,\mathrm{min}$.

Since we have no exact solution for comparison with our simulation results, we compute the L^2-distance between the concentration field obtained for a given resolution and the one obtained with the finest resolution in our numerical experiments ($h = 1/512$). This can give us empirical proof about the stability of the method.

L^2-distance	$\Delta t = 0.4$	$\Delta t = 0.2$	$\Delta t = 0.1$
$h = 1/64$	0.91	0.53	0.31
$h = 1/128$	0.60	0.39	0.23
$h = 1/256$	0.28	0.18	0.12

The results shown in this table display the stability of the method.

4.2. Numerical simulation of the motion of many cells subject to chemotaxis

The objective of this test problem is to assess the stability of the numerical method we have established when many cells are interacting with the chemoattractant and with other cells.

We adopt here the same setup as that in the previous paragraph, except we now place initially 14 cells in a domain extended in size to accommodate them all. The concentration of chemoattractant satisfies the same PDE as before, with identical boundary conditions.

In order to avoid the collisions of cells, we use a short-ranged repelling force [20]. Details on the actual implementation are provided in Appendix

Appendix C. The range of the force is of order $\mathcal{O}(h)$ which ensures that it shrinks to zero as $h \to 0$. In practise, we chose $\rho = 2\sqrt{2}h$, in order to keep a minimal distance between two cells corresponding to a line of four triangular elements. Figure 5 shows a realisation of this simulation.

5. Conclusion

We would like to recall a last time the main characteristics of the approach we have developed in this paper:

- The cells are discrete non deformable solid entities and no longer modelled as point particles;
- The evolution of the concentration of extracellular chemicals satisfies an advection-reaction-diffusion equation; a mixed finite element method is adopted to better monitor fluxes of chemicals, especially through the membrane of cells.
- The membrane of cells is modelled mathematically and effectively delimits the bulk and the cytosol;
- Internal variables allow the management of the interface, of the fluxes of chemicals through the membrane of cells, and allow the coupling of the motion of cells with the external stimuli received by the cells through its membrane
- Our simulation framework is highly modular, allowing to couple easily different models of different nature;
- The computational cost of the simulation is contained thanks to the fictitious domain method. This framework can fit many cells: indeed, the cost in terms of degrees of freedom for the boundary of cells grows linearly with the cumulated perimeter of the cells.

In section 4, we have provided two possible realisations of this simulation set up in a classical chemotaxis example: first with one cell and finally with several cells in the computational domain. To avoid collisions between cells, we implemented a short-range repulsive force acting between cells.

Possible future works include the testing of this framework against a realistic biological situation, for instance [19] or [33]. Another possible direction would be adding intracellular spatial chemical dynamics to better understand the signal transduction process in the cell.

Appendix A. Efficient computation of operators specific to fictitious domain method

The fictitious domain method allows the use of a single regular mesh for the computation of the solution of a PDE on a moving domain, whereas other methods, for instance ALE, would often involve costly remeshing and interpolation steps. However, this method still requires us to enforce the geometry of the problem, through the Lagrange multiplier. Since at each time step the cells change position, the geometry changes accordingly, so the operators involving the Lagrange multiplier space and the volume-supported spaces must be updated. The computation of those operators usually involve interpolating the interface on the regular mesh.

Let us make our point on an example. In Equation (11a), the Lagrange multiplier $\boldsymbol{\xi}$ appear in the dual pairing $\langle \boldsymbol{\xi}, \boldsymbol{w} \rangle$. The discretised version of this expression reads

$$\langle \boldsymbol{\xi}_h, \boldsymbol{w}_h \rangle = \int_{[0,1]} \boldsymbol{\xi}_h(s) \cdot \boldsymbol{w}_h(\boldsymbol{\gamma}(s)) \, \|\boldsymbol{\gamma}'(s)\| \, \mathrm{d}s, \tag{A.1}$$

for $\boldsymbol{w}_h \in \boldsymbol{W}_h.$, where we assumed γ to be a C^1-parametrisation of the interface. Since the functions $\boldsymbol{w}_h$ have all a small compact support, formed by the set of triangles to which the degree of freedom associated to $\boldsymbol{w}_h$ belong, computing accurately this integral is not easy as it seems. A tailored procedure must be adopted so its cost remains reasonable.

Noticing that we can rewrite (A.1) as:

$$\langle \boldsymbol{\xi}_h, \boldsymbol{w}_h \rangle = \sum_{\substack{T \in \mathcal{T} \\ T \cap \mathcal{I}(t) \neq \emptyset}} \int_{T \cap \mathcal{I}(t)} \boldsymbol{\xi}_h \cdot \boldsymbol{w}_h \, \mathrm{d}s, \tag{A.2}$$

a possible approach takes advantage of the regularity of the mesh to compute the points of intersection of the interface with the edges of the triangles forming the mesh. On Figure A.6, those points, numbered from 1 to 6 quicky allow us to find the triangles supporting the interface. They are the solution of the equations of unknown s of

$$\left(\boldsymbol{\gamma}(s) - \begin{Bmatrix} (ih, 0)^\top \\ (0, jh)^\top \\ \frac{1}{2}(kh, kh)^\top \end{Bmatrix} \right) \cdot \begin{Bmatrix} (1,0)^\top \\ (0,1)^\top \\ (1,1)^\top \end{Bmatrix} = 0, \tag{A.3}$$

defining for suitable integers i, j, k the intersection of $\mathcal{I}(t)$ with the edges of the triangles of the mesh.

On Figure (A.6), after point 2 on segment $[j,k]$ and 3 on segment $[k,i]$ have been computed, then immediately one deduces that the arc $\widehat{2,3}$ is included in triangle ijk. We deduce also that degrees of freedom associated to nodes i, j and k are not part of the annihilator of the Lagrange multiplier space.

Let $p_1, p_2, \ldots, p_M$, with $M \in \mathbb{N}$ be the solutions of Equation (A.3) arranged in increasing order. Also let us recall that $\boldsymbol{\xi}_h$ is an element of $\boldsymbol{\Xi}_h$, hence is supported on some part $I \in \mathcal{I}_h$ of the interface. Let us denote by r, s the curvilinear parameters such that $[r,s] = \boldsymbol{\gamma}^{-1}(I)$, then Equation (A.2) becomes:

$$\langle \boldsymbol{\xi}_h, \boldsymbol{w}_h \rangle = \sum_{\substack{1 \le i \le M \\ (p_i, p_{i+1}) \cap (r,s) \neq \emptyset}} \int_{\max(p_i, r)}^{\min(p_{i+1}, s)} \boldsymbol{\xi}_h(t) \cdot \boldsymbol{w}_h(\boldsymbol{\gamma}(t)) \, \|\boldsymbol{\gamma}'(t)\| \, \mathrm{d}t. \qquad \text{(A.4)}$$

This leads us to write the procedure 1 for the efficient computation of discretised fictitious domain operators. It allows looping through the segments of the interface and the points of intersection of the interface and the grid only once. Moreover, since the interface $\mathcal{I}(t)$ is composed of N non-intersecting connected components, this procedure can be easily parallelised to take advantage of modern computing architectures.

We can also deduce a procedure to compute efficiently the discretised version X of the characteristic function χ_t of the cells, *i.e.* $\chi_t(\boldsymbol{x}) = 1$ if $\boldsymbol{x} \in \bigcup C_j(t)$, and 0 otherwise. We write, for a given ϕ_k basis function of one of the approximation spaces, supported on the triangle T:

$$X_k = \int_T \chi_t \, \phi_k \, \mathrm{d}\Omega \approx \frac{1}{T} \int_T \chi_t \, \mathrm{d}\Omega \times \int_T \phi_k \, \mathrm{d}\Omega. \qquad \text{(A.5)}$$

Indeed, from Figure A.6, it is easy to find all triangles strictly inside or outside the area of the cells, by taking advantage of the convexity of cells.

For a triangle cut through by the interface, then we can approximate the integral $\int_{T \cap (\bigcup C_j)} \chi_t \, \mathrm{d}\Omega$ by evaluating the area of the sub-triangle formed by the points of intersection of the interface with the edges of this triangle and the vertex at the intersection of those two edges: for instance, on Figure A.6, we would evaluate the area of the sub-triangles $j12$, $2k3$, $3k4$, $4k5$. After determining whether this sub-triangle is inside or outside the cell, then we easily compute the value of the above integral.

Algorithm 1 Computation of discretised fictitious domain operators

procedure ComputeFictitiousOperator
  $o_1 \leftarrow \min \boldsymbol{\gamma}^{-1}(I_1),\ o_2 \leftarrow \min \boldsymbol{\gamma}^{-1}(I_2), \ldots,\ o_L \leftarrow \min \boldsymbol{\gamma}^{-1}(I_L)$
  Get $p_1, p_2, \ldots, p_M$, by solving Equation (A.3).
  Initialise matrix operator A.
  $i \leftarrow 1$
  $j \leftarrow 1$
  while $i \leq M$ **do**
    if $o_{j+1} \leq p_i$ **then** ▷ $(o_j, o_{j+1}) \cap (p_i, p_{i+1}) = \emptyset$
      $j \leftarrow j + 1$
    end if
    if $p_{i+1} \leq o_j$ **then** ▷ $(o_j, o_{j+1}) \cap (p_i, p_{i+1}) = \emptyset$
      $i \leftarrow i + 1$
    end if
    Select triangle K including segment $[\boldsymbol{\gamma}(p_i), \boldsymbol{\gamma}(p_{i+1})]$.
    for all nodes α of T **do**
      $A_{\alpha j} \leftarrow A_{\alpha j} + QuadratureRule(\max(p_i, o_j), \min(p_{i+1}, o_{j+1}))$
    end for
    if $[p_i, p_{i+1}] \subset (o_j, o_{j+1})$ **then**
      $i \leftarrow i + 1$
    else if $[o_j, o_{j+1}] \subset (p_i, p_{i+1})$ **then**
      $j \leftarrow j + 1$
    else if $p_i \in [o_j, o_{j+1}]$ & $p_{i+1} \notin [o_j, o_{j+1}]$ **then**
      $j \leftarrow j + 1$
    else if $p_i \notin [o_j, o_{j+1}]$ & $p_{i+1} \in [o_j, o_{j+1}]$ **then**
      $i \leftarrow i + 1$
    end if
  end while
  return A
end procedure

Appendix B. Preconditioning

The simulation of the chemotactic system presented in this paper requires the computation of the solution of very large sparse linear systems, using iterative methods such as `MinRes` or `GMRes`. When running, most of the CPU time is spent on such tasks, hence it is vital to equip those linear systems with competitive preconditioners that will reduce the number of iterations to achieve the required tolerance and its dependence to the grid size. The linear systems (21) and (22) are both saddle-point linear systems, they are of the form:

$$\begin{bmatrix} A & B^\top \\ B & 0 \end{bmatrix} \begin{bmatrix} x_1 \\ x_2 \end{bmatrix} = \begin{bmatrix} y_1 \\ y_2 \end{bmatrix}, \tag{B.1}$$

where A is symmetric positive definite and B rectangular. In [3], Benzi reviews the different available methods to efficiently preconditioning such systems. More specifically, on the preconditioning of saddle-point linear systems arising in computational fluid dynamics, an extensive litterature is our disposal.

In [32, 11], Silvester *et al.* and Elman *et al.* propose block preconditioners for linear systems of incompressible Navier-Stokes equations. The solution to $Ax = y$ is approximated using a multigrid approach and the second block is usually an approximation of the Schur complement, so the preconditioner takes the following form:

$$\mathcal{P}^{-1} = \begin{bmatrix} \texttt{multigrid}(A) & 0 \\ 0 & \tilde{S}^{-1} \end{bmatrix} \tag{B.2}$$

Because of the presence of the Lagrange multiplier, the block B is the concatenation of the discretised gradient operator and the discretised Lagrange multiplier operator:

$$B^\top = \begin{bmatrix} \nabla \\ \Lambda^\top \end{bmatrix} \tag{B.3}$$

where $\nabla \in \mathbb{R}^{n_1 \times M}$, $\Lambda^\top \in \mathbb{R}^{n_2 \times M}$ and $n_1 \gg n_2$.

The block $\tilde{S}$ has block diagonal structure as follows:

$$\tilde{S} = \begin{bmatrix} \tilde{S}_1 & \\ & \tilde{S}_2 \end{bmatrix} \tag{B.4}$$

For $\tilde{S}_1$, we can make use of the BFBt preconditioner introduced by Silvester. For $\tilde{S}_2$, usually the mass matrix of the Lagrange multiplier space yields good

results [3]. We will not discuss in more details the effectiveness of the preconditioners since it is not in the scope of this paper.

Appendix C. Avoiding collision of cells

To prevent the overlap of two cells whilst minimising the bias introduced in the simulation, we use a short-ranged repulsive force which model is described in [20]. In the case of two circular cells of radius r_i and r_j repelling each other, the expression of this (artificial) force reads:

$$\boldsymbol{F}_{i\to j} = \frac{F_0}{\epsilon_c}\left[\min\left(\frac{\|\boldsymbol{x}_i-\boldsymbol{x}_j\|-r_i-r_j-\rho}{\rho},0\right)\right]^2 \frac{(\boldsymbol{x}_i-\boldsymbol{x}_j)}{\|\boldsymbol{x}_i-\boldsymbol{x}_j\|} \tag{C.1}$$

where F_0 is the typical value of the forces acting on the cells and ρ represents the range of the repulsive force. When the two spherical cells see their distance shrinking to ρ or less, the value of the repulsive force between the two cells becomes nonzero. Parameter ϵ_c a dimensionless parameter of order $\epsilon_c = \mathcal{O}\left(\left(\frac{\delta}{\rho}\right)^2\right)$, where δ is the penetration length.

In the case of arbitrary shaped cells, a moment of force also arises. The force applied by one cell on another reads:

$$\boldsymbol{F}_{i\to j} = \int_{C_i}\int_{C_j} \frac{F_0}{\epsilon_c}\left[\min\left(\frac{\|\boldsymbol{x}_1-\boldsymbol{x}_2\|-\rho}{\rho},0\right)\right]^2 \frac{(\boldsymbol{x}_1-\boldsymbol{x}_2)}{\|\boldsymbol{x}_1-\boldsymbol{x}_2\|}\,\mathrm{d}\boldsymbol{x_1}\,\mathrm{d}\boldsymbol{x_2} \tag{C.2}$$

and the moment of force:

$$\begin{aligned}\boldsymbol{M}_{i\to j} = \int_{C_i}\int_{C_j} \frac{F_0}{\epsilon_c}&\left[\min\left(\frac{\|\boldsymbol{x}_1-\boldsymbol{x}_2\|-\rho}{\rho},0\right)\right]^2 \\ &\frac{(\boldsymbol{x}_1-\boldsymbol{x}_2)}{\|\boldsymbol{x}_1-\boldsymbol{x}_2\|}\times(\boldsymbol{x}_1-\boldsymbol{x}_i)\,\mathrm{d}\boldsymbol{x_1}\,\mathrm{d}\boldsymbol{x_2}.\end{aligned} \tag{C.3}$$

Numerically, this is an expensive work to compute those two integrals accurately, however, such a precision is not needed for the purpose we are after and we could be contented with a approximation that would still prevent the cells from colliding. We opt for a one-point integration approximation as shown on Figure C.8 and write:

$$\boldsymbol{F}_{i\to j} = \frac{F_0}{\epsilon_c}\left[\min\left(\frac{d_{ij}-\rho}{\rho},0\right)\right]^2 \frac{(\boldsymbol{x}_i-\boldsymbol{x}_j)}{\|\boldsymbol{x}_i-\boldsymbol{x}_j\|}. \tag{C.4}$$

To compute a reasonable approximation of the moment of force, a two-point approximation scheme is used as shown on Figure C.9 in the case of elliptic cells. The expression for the moment then reads:

$$\boldsymbol{M}_{i\to j} = \sum_{k,l} \frac{F_0}{\epsilon_c} \left[\min\left(\frac{d_{ijkl} - \rho}{\rho}, 0 \right) \right]^2 \frac{(\boldsymbol{f}_{ik} - \boldsymbol{f}_{jl})}{\|\boldsymbol{f}_{ik} - \boldsymbol{f}_{jl}\|} \times (\boldsymbol{f}_{ik} - \boldsymbol{x}_i). \qquad \text{(C.5)}$$

When computing this approximation, four distances must be computed and they are the main cost in the computation of the moment.

Acknowledgement

This publication was based on work supported in part by Award No KUK-C1-013-04 , made by King Abdullah University of Science and Technology (KAUST).
The research leading to these results has received funding from the European Research Council under the *European Community*s Seventh Framework Programme (*FP7/2007-2013*)/ ERC *grant agreement* No. 239870. Radek Erban would also like to thank Brasenose College, University of Oxford, for a Nicholas Kurti Junior Fellowship; the Royal Society for a University Research Fellowship; and the Leverhulme Trust for a Philip Leverhulme Prize.

References

[1] M. Alber, N. Chen, P.M. Lushnikov, and S.A. Newman. Continuous macroscopic limit of a discrete stochastic model for interaction of living cells. *Physical review letters*, 99(16):168102, 2007.

[2] B. Alberts. *Molecular biology of the cell: Reference edition*. Number vol. 1 in Molecular Biology of the Cell: Reference Edition. Garland Science, 2008.

[3] M. Benzi, G.H. Golub, and J. Liesen. Numerical solution of saddle point problems. *Acta numerica*, 14(1):1–137, 2005.

[4] J.T. Bonner and LJ Savage. Evidence for the formation of cell aggregates by chemotaxis in the development of the slime mold dictyostelium discoideum. *Journal of Experimental Zoology*, 106(1):1–26, 1947.

[5] M. Brenner, L. Levitov, and E. Budrene. Physical mechanisms for chemotactic pattern formation by bacteria. *Biophysical Journal*, 74(4):1677–1693, 1998.

[6] D. Bresch, V. Calvez, E. Grenier, P. Vigneaux, JF Gerbeau, A. Decoene, A. Lorz, S. Martin, B. Maury, and M. Tang. Simulation of self-propelled chemotactic bacteria in a stokes flow. In *ESAIM: Proceedings*, volume 30, pages 104–123. EDP Sciences, 2010.

[7] J. Buhl, DJT Sumpter, ID Couzin, JJ Hale, E. Despland, ER Miller, and SJ Simpson. From disorder to order in marching locusts. *Science*, 312(5778):1402–1406, 2006.

[8] F. Collino, P. Joly, and F. Millot. Fictitious domain method for unsteady problems. *Journal of Computational Physics*, 138(2):907–938, 1997.

[9] J.C. Dallon and H.G. Othmer. A continuum analysis of the chemotactic signal seen bydictyostelium discoideum. *Journal of theoretical biology*, 194(4):461–483, 1998.

[10] M. Eisenbach. Sperm chemotaxis. *Reviews of reproduction*, 4(1):56–66, 1999.

[11] H.C. Elman, D.J. Silvester, and A.J. Wathen. Block preconditioners for the discrete incompressible navier–stokes equations. *International journal for numerical methods in fluids*, 40(3-4):333–344, 2002.

[12] R. Erban. *From individual to collective behaviour in biological systems*. PhD thesis, University of Minnesota, 2005.

[13] R. Erban, I.G. Kevrekidis, and H.G. Othmer. An equation-free computational approach for extracting population-level behavior from individual-based models of biological dispersal. *Physica D: Nonlinear Phenomena*, 215(1):1–24, 2006.

[14] R. Erban and H.G. Othmer. From individual to collective behavior in bacterial chemotaxis. *SIAM Journal on Applied Mathematics*, pages 361–391, 2004.

[15] R. Erban and H.G. Othmer. From signal transduction to spatial pattern formation in e. coli: a paradigm for multiscale modeling in biology. *Multiscale Modeling and Simulation*, 3(2):362–394, 2005.

[16] R. Erban and H.G. Othmer. Taxis equations for amoeboid cells. *Journal of mathematical biology*, 54(6):847–885, 2007.

[17] M. Flegg, J. Chapman, and R. Erban. The two-regime method for optimizing stochastic reaction-diffusion simulations. *Journal of the Royal Society Interface*, 9(70):859–868, 2012.

[18] B. Franz and R. Erban. Hybrid modelling of individual movement and collective behaviour. In *Dispersal, individual movement and spatial ecology: A mathematical perspective*. Springer-Verlag, 2012.

[19] P. Friedl, Y. Hegerfeldt, M. Tusch, et al. Collective cell migration in morphogenesis and cancer. *International Journal of Developmental Biology*, 48:441–450, 2004.

[20] R. Glowinski, TW Pan, TI Hesla, DD Joseph, and J. Periaux. A fictitious domain approach to the direct numerical simulation of incompressible viscous flow past moving rigid bodies: application to particulate flow. *Journal of Computational Physics*, 169(2):363–426, 2001.

[21] R. Glowinski, T.W. Pan, and J. Periaux. A fictitious domain method for dirichlet problem and applications. *Computer Methods in Applied Mechanics and Engineering*, 111(3-4):283–303, 1994.

[22] R. Glowinski, TW Pan, and J. Periaux. Distributed lagrange multiplier methods for incompressible viscous flow around moving rigid bodies. *Computer methods in applied mechanics and engineering*, 151(1):181–194, 1998.

[23] R. Glowinski, TW Pan, R.O. Wells, and X. Zhou. Wavelet and finite element solutions for the neumann problem using fictitious domains. *Journal of Computational Physics*, 126(1):40–51, 1996.

[24] P. Joly and L. Rhaouti. Domaines fictifs, éléments finis h (div) et condition de neumann: le probleme de la condition inf-sup. *Comptes Rendus de l'Académie des Sciences-Series I-Mathematics*, 328(12):1225–1230, 1999.

[25] E.F. Keller and L.A. Segel. Model for chemotaxis. *Journal of Theoretical Biology*, 30(2):225–234, 1971.

[26] H. Levine, D.A. Kessler, and W.J. Rappel. Directional sensing in eukaryotic chemotaxis: a balanced inactivation model. *Proceedings of the National Academy of Sciences*, 103(26):9761, 2006.

[27] N.V. Mantzaris, S. Webb, and H.G. Othmer. Mathematical modeling of tumor-induced angiogenesis. *Journal of Mathematical Biology*, 49(2):111–187, 2004.

[28] B. Maury. Direct simulations of 2d fluid-particle flows in biperiodic domains. *Journal of computational physics*, 156(2):325–351, 1999.

[29] C.A. Parent and P.N. Devreotes. A cell's sense of direction. *Science*, 284(5415):765–770, 1999.

[30] GJ Pettet, HM Byrne, DLS McElwain, and J. Norbury. A model of wound-healing angiogenesis in soft tissue. *Mathematical biosciences*, 136(1):35–63, 1996.

[31] P. Raviart and J. Thomas. A mixed finite element method for 2-nd order elliptic problems. *Mathematical aspects of finite element methods*, pages 292–315, 1977.

[32] D. Silvester, H. Elman, D. Kay, and A. Wathen. Efficient preconditioning of the linearized navier–stokes equations for incompressible flow. *Journal of Computational and Applied Mathematics*, 128(1):261–279, 2001.

[33] A.J. Singer, RA Clark, et al. Cutaneous wound healing. *N Engl J Med*, 341(10):738–746, 1999.

[34] T. Vicsek, A. Czirók, E. Ben-Jacob, I. Cohen, and O. Shochet. Novel type of phase transition in a system of self-driven particles. *Physical Review Letters*, 75(6):1226–1229, 1995.

[35] C. Xue, H. Hwang, K. Painter, and R. Erban. Travelling waves in hyperbolic chemotaxis equations. *Bulletin of Mathematical Biology*, 73(8):1695–1733, 2011.

[36] C. Xue and H. Othmer. Multiscale models of taxis-driven patterning in bacterial populations. *SIAM Journal on Applied Mathematics*, 70(1):133–167, 2009.

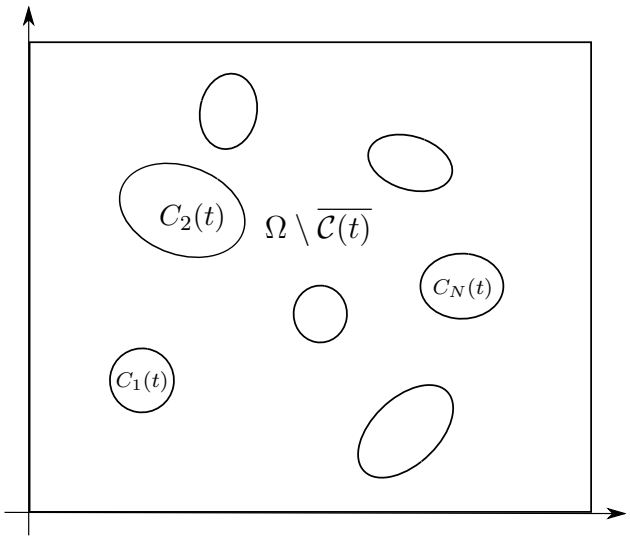

Figure 1: Cavity Ω and cells $C_i(t)$

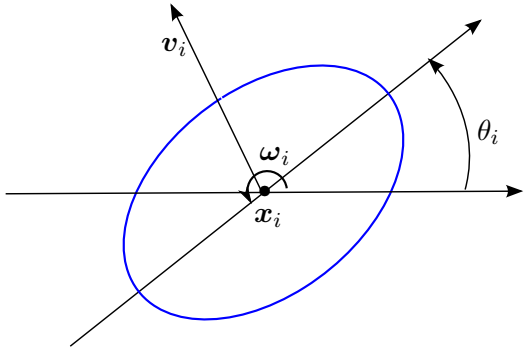

Figure 2: Kinematic parameters characterising the movement of a cell of a given shape (here elliptic).

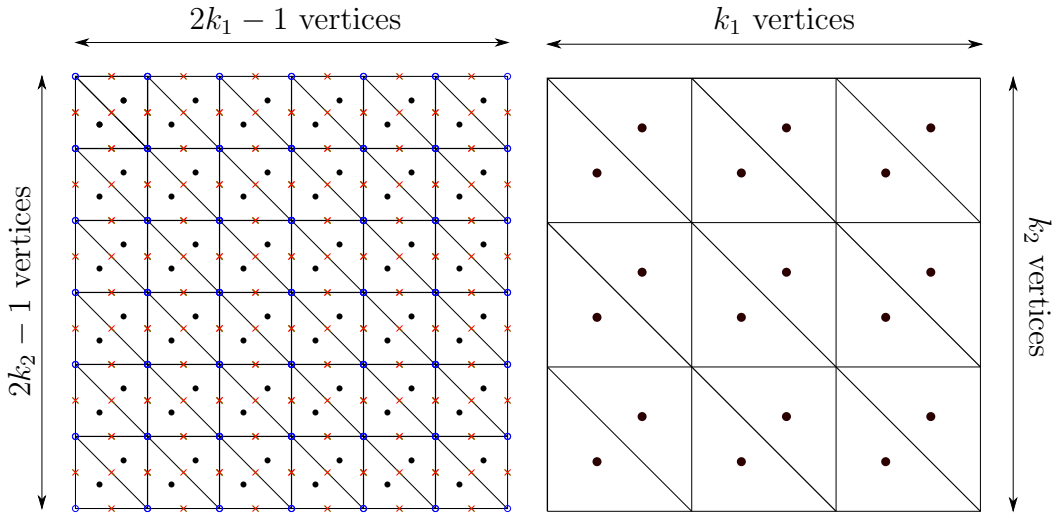

(a) Mesh for the densities, density fluxes and velocity.

(b) Mesh for the pressure

Figure 3: The two meshes used for the discretisation of the cavity Ω. On the left-hand side picture, the degrees of freedom for the velocity field are shown in blue dots, the densities in black dots and the density fluxes in red crosses. On the right-hand side picture, the black dots represent the location of the degrees of freedom for the pressure field.

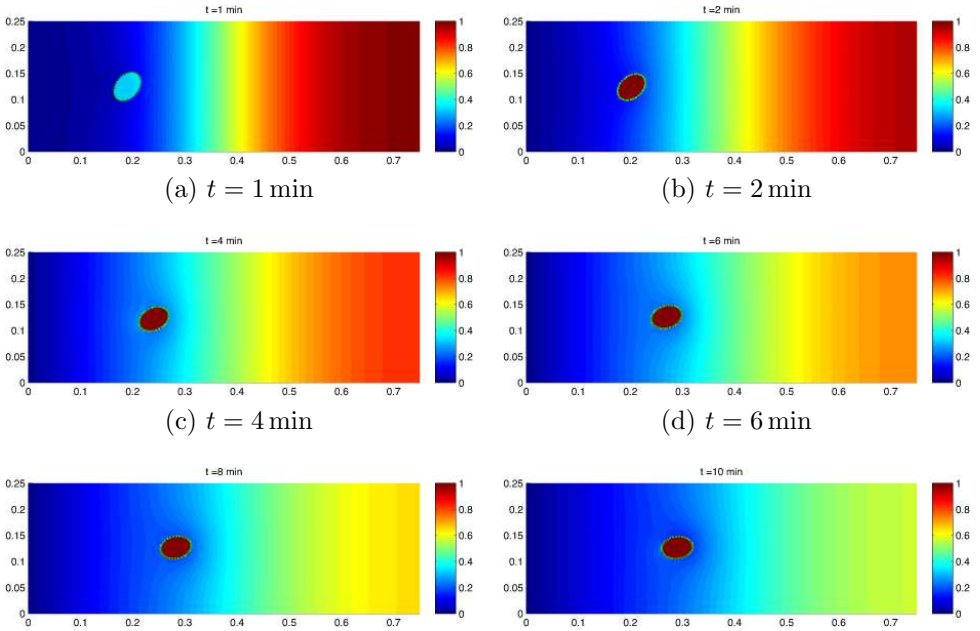

(a) $t = 1\,\text{min}$ (b) $t = 2\,\text{min}$

(c) $t = 4\,\text{min}$ (d) $t = 6\,\text{min}$

(e) $t = 8\,\text{min}$ (f) $t = 10\,\text{min}$

Figure 4: Simulation of the motion of one cell undergoing chemotaxis by a single chemoattractant.

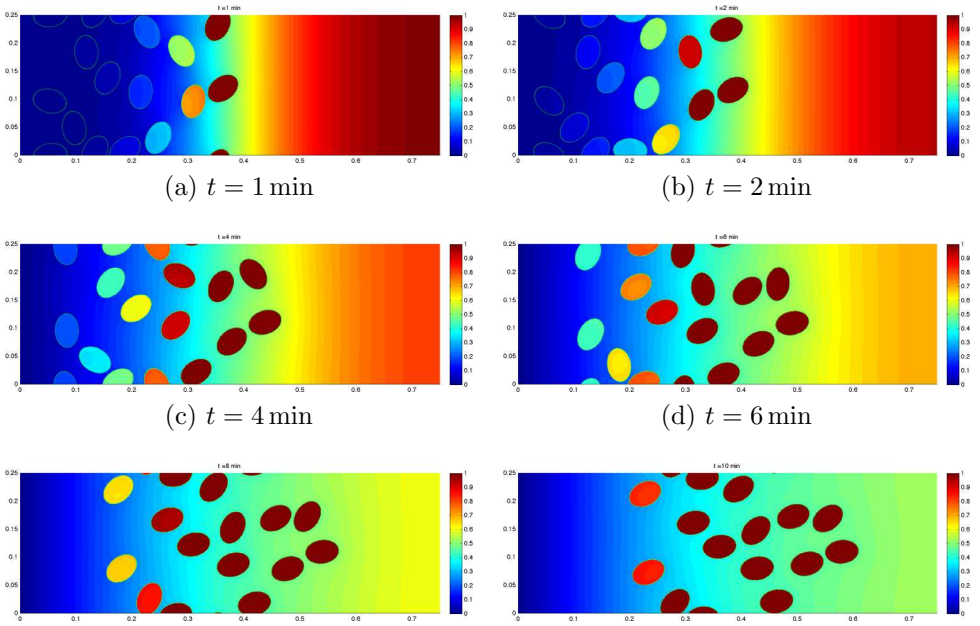

(a) $t = 1\,\text{min}$ (b) $t = 2\,\text{min}$

(c) $t = 4\,\text{min}$ (d) $t = 6\,\text{min}$

(e) $t = 8\,\text{min}$ (f) $t = 10\,\text{min}$

Figure 5: Simulation of the motion of 14 cells undergoing chemotaxis by a single chemoattractant. The colour indicates the local concentration of chemoattractant (red means 'high' and blue means 'low'). The gradual change in colour of the cells in time shows the absorption of the chemoattractant by the cells. The initial position of the cells is random in the left-hand part of the domain. Videos of this simulation are available as supplementary data for this paper.

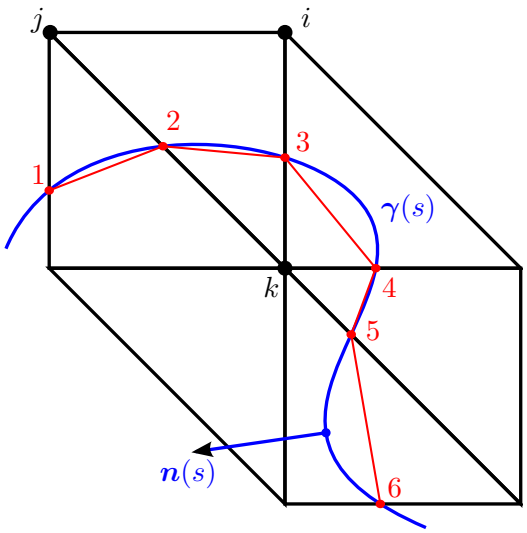

Figure A.6

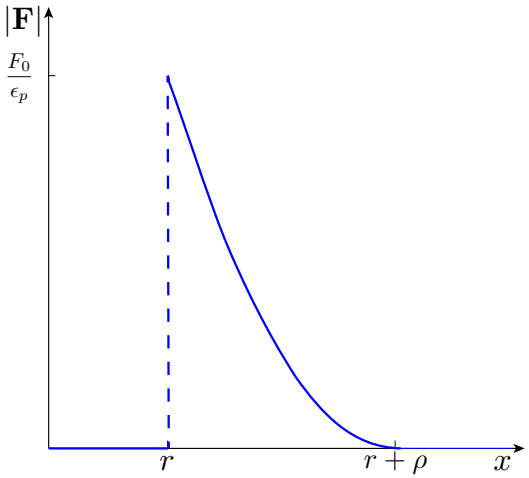

Figure C.7: Sketch of the modulus of the repulsive force in 1D for a cell centred in 0 and of radius r. The range of the force is ρ.

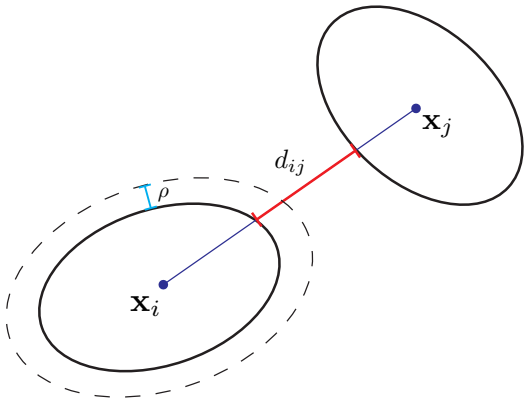

Figure C.8: This figure shows how the force $\boldsymbol{F}_{i\to j}$ is computed: the length d_{ij} is the distance between the points of intersection of the line $(\boldsymbol{x}_i, \boldsymbol{x}_j)$ with the boundary of each cell.

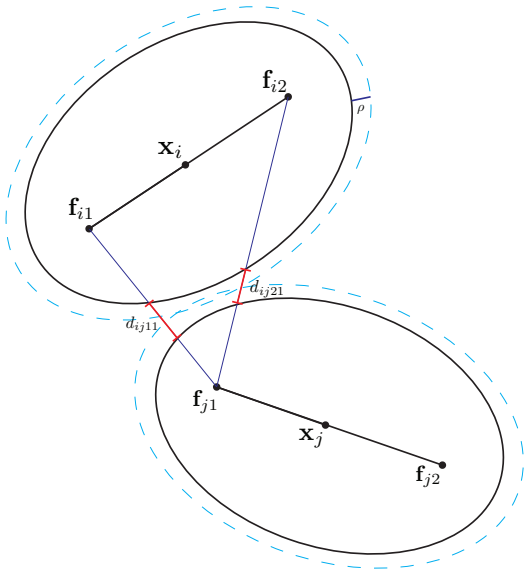

Figure C.9: This figure shows how the moment $\boldsymbol{M}_{i\to j}$ is computed: using the foci of each ellipse, a elementary moment is calculated with respect to the centre of each ellipse.

RECENT REPORTS

12/24	Correspondence between one- and two-equation models for solute transport in two-region heterogeneous porous media	Davit Wood Debenest Quintard
12/25	Rolie-Poly fluid flowing through constrictions: Two distinct instabilities	Reis Wilson
12/26	Age related changes in speed and mechanism of adult skeletal muscle stem cell migration	Collins-Hooper Woolley Dyson Patel Potter Baker Gaffney Maini Dash Patel
12/27	The interplay between tissue growth and scaffold degradation in engineered tissue constructs	ODea Osborne El Haj Byrne Waters
12/28	Non-linear effects on Turing patterns: time oscillations and chaos.	Aragon Barrio Woolley Baker Maini
12/29	Colorectal Cancer Through Simulation and Experiment	Kershaw Byrne Gavaghan Osborne
12/30	A theoretical investigation of the effect of proliferation and adhesion on monoclonal conversion in the colonic crypt	Mirams Fletcher Maini Byrne
12/31	Convergent evolution of spiny mollusk shells points to elastic energy minimum	Chirat Moulton Shipman Goriely
12/32	Three-dimensional oblique water-entry problems at small deadrise angles	Moore Howison Ockendon Oliver
12/33	Second weak order explicit stabilized methods for stiff stochastic differential equations	Abdulle Vilmart Zygalakis
12/34	The sensitivity of Graphene ‘Snap-through’ to substrate geometry	Wagner Vella

12/38	Dispersal and noise: Various modes of synchrony in ecological oscillators	Bressloff Lai
12/39	Boundary conditions for free surface inlet and outlet problems	Taroni Breward Howell Oliver
12/40	A Branch and Bound Algorithm for the Global Optimization of Hessian Lipschitz Continuous Functions	Fowkes Gould Farmer
12/41	The Orthogonal Gradients Method: a Radial Basis Functions Method for Solving Partial Differential Equations on Arbitrary Surfaces	Piret
12/42	Squeeze-Film Flow in the Presence of a Thin Porous Bed, with Application to the Human Knee Joint	Knox Wilson Duffy McKee
12/43	Gravity-driven draining of a thin rivulet with constant width down a slowly varying substrate	Paterson Wilson Duffy
12/44	The 'Sticky Elastica': Delamination blisters beyond small deformations	Wagner Vella
12/45	Stochastic models of intracellular transport	Bressloff Newby
12/46	The effects of noise on binocular rivalry waves: a stochastic neural field model	Webber Bressloff
12/47	An Ensemble Bayesian Filter for State Estimation	Farmer

Copies of these, and any other OCCAM reports can be obtained from:

Oxford Centre for Collaborative Applied Mathematics
Mathematical Institute
24 - 29 St Giles'
Oxford
OX1 3LB
England
www.maths.ox.ac.uk/occam